Investigation into the Control Methods to Reduce the DC-Link Capacitor Ripple Current in a Back-to-Back Converter

Qin, Zian; Wang, Huai; Blaabjerg, Frede; Loh, Poh Chiang

Published in:
Proceedings of the 2014 IEEE Energy Conversion Congress and Exposition (ECCE)

DOI (link to publication from Publisher):
10.1109/ECCE.2014.6953395

Publication date:
2014

Document Version
Early version, also known as pre-print

Digital Object Identifier (DOI):

Proceedings of the IEEE Energy Conversion Congress and Exposition (ECCE 2014), Pittsburgh, PA, USA, 14-18 September, 2014.

Investigation into the Control Methods to Reduce the DC-Link Capacitor Ripple Current in a Back-to-Back Converter

Zian Qin
Huai Wang
Frede Blaabjerg
Poh Chiang Loh

Suggested Citation

Z. Qin, H. Wang, F. Blaabjerg, and P. C. Loh, “Investigation into the control methods to reduce the DC-link capacitor ripple current in a back-to-back converter," *in Proc. IEEE Energy Convers. Congr. and Expo.*, 2014, pp. 203-210.

Investigation into the Control Methods to Reduce the DC-Link Capacitor Ripple Current in a Back-to-Back Converter

Zian Qin, Huai Wang, *Member, IEEE*, Frede Blaabjerg, *Fellow, IEEE*, Poh Chiang Loh, *Senior Member, IEEE*
Department of Energy Technology, Aalborg University
9220 Aalborg, Denmark
zqi@et.aau.dk, hwa@et.aau.dk, fbl@et.aau.dk, pcl@et.aau.dk

***Abstract*—Three-phase back-to-back converters have a wide range of applications (e.g. wind turbines) in which the reliability and cost-effectiveness are of great concern. Among other components and interconnections, DC-link capacitors are one of the weak links influenced by environmental stresses (e.g. ambient temperature, humidity, etc.) and operating stresses (e.g. voltage, ripple current). This paper serves to investigate the ways of reducing ripple current stresses of DC-link capacitors in back-to-back converters. The outcome could benefit to achieve either an extended lifetime for a designed DC-link or a reduced DC-link size for fulfilling a specified lifetime target. The proposed control strategies have been demonstrated on a study case of a 1.5 kW converter prototype. The experimental verifications are in well agreement with the theoretical analyses.**

I. Introduction

It has been observed in recent years that the challenges in power electronics design is in a way of more demanding reliability performance and more stringent cost constraint [1–3], such as the pressure of cost-of-energy reduction in renewable energies. Three-phase voltage-source Back-to-Back (BTB) converters are widely used in wind turbines, of which the DC-link capacitors are found to be one of the weak links in field operations. Both aluminum electrolytic capacitors and film capacitors have been designed into different wind turbine products. For aluminum electrolytic capacitors, the ambient temperature and the internal temperature rise due to ripple current are of critical stressors that influence the lifetime. For film capacitors, the reliability performance is still of a high level of uncertainty in field operation due to relatively lack of field experiences. In high ripple current stress scenarios, high internal temperature raises could still occur. Moreover, the internal temperature variations will induce more chance of moisture absorption, which is a critical stressor to the failure of film capacitors [4]. The capacitor lifetime dependence on temperature and voltage has been discussed in [4] and is represented in (1), where L is the lifetime, V is maximum voltage across capacitors, K_B is Boltzmanns constant (8.62×10^{-5} eV/K), E_a is activation energy, n is the voltage stress exponent, T is the hotspot temperature, T_{amb} is the ambient temperature, R_{ha} is the equivalent thermal resistance from hotspot to ambient, $ESR(f_i)$ is the equivalent series resistance at frequency f_i, $I_{rms}(f_i)$ is the root-mean-square value of the ripple current at frequency f_i. It can be noted that the ripple current spectrum contributes to the hotspot temperature in terms of self-heating of the capacitors. Therefore, the reduction of ripple current stresses will be beneficial to improve the reliability or to reduce the size of DC links composed of either electrolytic capacitors or film capacitors, or both.

$$\begin{cases} L \propto V^{-n} \times exp\left(\frac{E_a}{K_B T}\right) \\ T = T_{amb} + R_{ha} \times \sum_{i=1}^{n} ESR(f_i) \times I_{rms}^2(f_i) \end{cases} \quad (1)$$

Efforts have been devoted to the reduction of ripple current stresses of capacitors in three-phase systems in the prior-art research [5–8]. Current source converters are used for the wind power system in order to avoid the DC link capacitor [5]. However the performance is not as good as voltage source converters in terms of the power loss caused by the DC link inductor and the quality of the current especially at low power ratio. The voltage source converter technology is much more mature and it is still the dominant in the market as well as in the research. The feed forward control and direct capacitor current control can be used to reduce the imbalance between the input and output power of the DC link capacitor during the dynamic process [6], [8]. However, the approaches cannot handle the ripple current with a carrier frequency on the DC link, which is introduced by the PWM modulation and exists during both the dynamic and steady state.

The research focusing on the carrier frequency ripple current has therefore be conducted [9–15]. The RMS value of the DC capacitor current is derived for a AC-DC-AC system with a diode rectifier in front [9]. The analytical result has a good accuracy even the ac currents contain high ripples. However the spectrum of the DC link current is a more critical factor for the DC link capacitor due to its frequency-dependent $ESR(f_i)$ [16]. The spectrum of the DC link current in PWM converters has been derived for a single leg and three-phase systems, respectively [10], [11], [12], which actually contains DC component, baseband harmonics, carrier frequency harmonics, and carrier-sideband harmonics. However, only the DC capacitor current in a single stage power converter is analyzed, while that in a BTB converter is still unknown. Another important aspect is the approaches to reduce the DC capacitor current. Synchronizing the carriers of the back-to-back converter is an efficient way to reduce the DC-link current, where the in-phase condition is found to be the most optimal [7]. However, more

978-1-4799-5776-7/14/$31.00

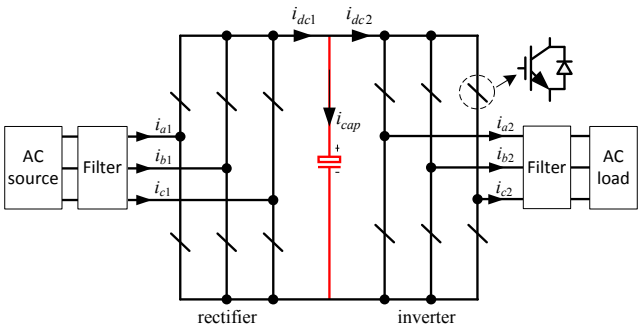

Fig. 1. Scheme of the back-to-back converter.

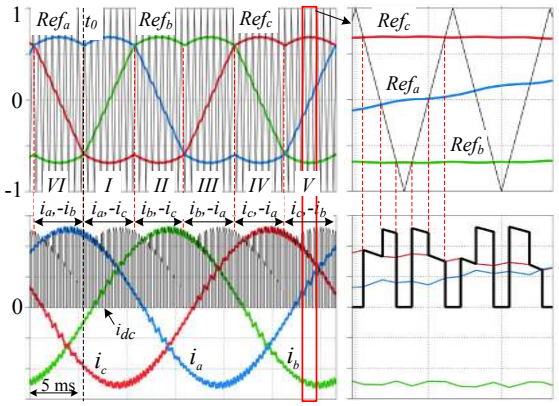

Fig. 2. Illustration of the converter side dc current.

details are still missing, and the impact of the other parameters is also worthy to be studied.

Therefore, in this paper the impact of the parameters on the DC link current as well as the DC capacitor current is investigated based on a simple derivation. Then the opportunities of using control strategies to reduce the DC capacitor current can be created. The analytical results are finally verified by the simulation results and the test on a 1.5 kW prototype in the laboratory.

II. Analysis of the DC Link Current

Fig. 1 demonstrates the scheme of a BTB converter, which is composed of a three-phase rectifier and a three-phase inverter. i_{ax}, i_{bx}, and i_{cx} are the AC currents, i_{dcx} is the DC link current, i_{cap} is the current of the DC link capacitor (x = 1 or 2, which represents the rectifier and the inverter, respectively). According to the Kirchhoff's Current Law, i_{cap} is the difference between i_{dc1} and i_{dc2}. It is therefore essential first to analyze the generation mechanism of i_{dcx}. In fact, as in a voltage source converter (the rectifier or the inverter), the i_{dcx} is the combination of i_{ax}, i_{bx} and i_{cx}. The switching between the AC currents finally leads to the pulsed i_{dcx}. A spectrum analysis is thus carried out for i_{dcx} in a universal three-phase voltage converter. The DC link current is illustrated in Fig. 2, where the Ref_a, Ref_b and Ref_c are the references of the modulation, i_a, i_b and i_c are the ac currents, which are expressed as follows,

$$\begin{cases} Ref_a = Mcos[\omega_0(t-t_0)] + M_{3rd} \\ Ref_b = Mcos[\omega_0(t-t_0) - \frac{2\pi}{3}] + M_{3rd} \\ Ref_c = Mcos[\omega_0(t-t_0) + \frac{2\pi}{3}] + M_{3rd} \end{cases} \tag{2}$$

$$\begin{cases} i_a = Icos[\omega_0(t-t_0) + \varphi] \\ i_b = Icos[\omega_0(t-t_0) - \frac{2\pi}{3} + \varphi] \\ i_c = Icos[\omega_0(t-t_0) + \frac{2\pi}{3} + \varphi] \end{cases} \tag{3}$$

where M is the modulation index, ω_0 is the fundamental frequency, M_{3rd} is the third-harmonic injection, I is the amplitude of the ac currents, φ is the power factor angle of the ac side, t_0 is the initial time, which is indicated in Fig. 2. It can be seen that, the dc link current has the same envelope with the ac currents. Moreover, according to the cross points of the references, a fundamental cycle is divided into six segments. In each segment the dc link current is composed of two ac currents, which are respectively the positive and minus currents in the phase of the top and bottom references. For example, in $Segment\ I$ since Ref_a and Ref_b are the top and bottom references, the dc link current i_{dc} is composed of i_a and i_b. In the zoomed figure, it is found that the dc link current is actually composed of four pulses in each switching cycle, where the amplitude is that of the corresponding ac current as mentioned above, while the durations of the current pulses are determined by the difference between the references. It should be noted that, the carrier-based SVPWM and the decreasing/increasing carrier are assumed to be employed, which can relieve the DC link ripple current according to the literatures [11]. The Fourier decomposition is then carried out for further analysis of the DC link current, and it can be represented by a double Fourier series as following [10],

$$\begin{aligned} i_{dc} &= I_0 + \sum_{n=1}^{\infty} I_n cos[n\omega_0(t-t_0) + \theta_n] \\ &+ \sum_{m=1}^{\infty}\sum_{n=-\infty}^{\infty} I_{mn} cos[(m\omega_s + n\omega_0)(t-t_0) + \theta_{mn}] \end{aligned} \tag{4}$$

where I_0 is the DC component, I_n and θ_n are the amplitude and initial phase of the fundamental and baseband harmonics, I_{mn} and θ_{mn} are the amplitude and initial phase of the carrier frequency and carrier-side harmonics, ω_s is the angular frequency of the carrier. It can be noted that the harmonics contain the components from fundamental frequency till carrier frequency multiplier. The dominant components however are the carrier frequency and carrier-sideband harmonics. Since the fundamental frequency of the DC link current is $3\omega_0$, their amplitudes can be derived as,

$$\begin{aligned} \frac{1}{2}I_{mn}^2 &= \frac{3\omega_0}{2\pi}\int_{t_0}^{t_0+\frac{2\pi}{3\omega_0}} i_{dc} i_{mn} dt = \frac{3\omega_0}{2\pi}\sum_{j=0}^{1}\sum_{k=0}^{N-1} \\ &\Big\{\Big(\int_{t_{01}+kT_s+jNT_s+t_o}^{t_{02}+kT_s+jNT_s+t_o} + \int_{t_{05}+kT_s+jNT_s+t_o}^{t_{06}+kT_s+jNT_s+t_o}\Big) i_1 \times i_{mn} dt + \\ &\Big(\int_{t_{02}+kT_s+jNT_s+t_o}^{t_{03}+kT_s+jNT_s+t_o} + \int_{t_{04}+kT_s+jNT_s+t_o}^{t_{05}+kT_s+jNT_s+t_o}\Big) i_2 \times i_{mn} dt\Big\} \end{aligned} \tag{5}$$

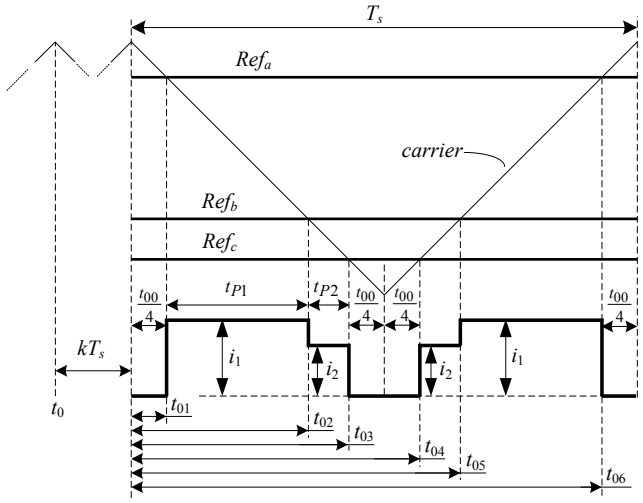

Fig. 3. Details of the DC link current in a switching cycle.

where $i_{mn} = I_{mn}cos[(m\omega_s+n\omega_0)(t-t_0)+\theta_{mn}]$, k means it is the $(k+1)^{th}$ switching cycle, $N = \frac{\omega_s}{6\omega_0}$, $t_{01} \sim t_{06}$ are the time durations regarding to the pulse currents as indicated in Fig. 3, i_1 and i_2 are the amplitudes of the pulse currents, $j = 0, 1$ represent $Segment\ I$ and II, respectively. By observing Fig. 3, it can be found that,

$$j=0,\begin{cases} i_1 = i_a \\ i_2 = -i_c \end{cases} \quad j=1,\begin{cases} i_1 = i_b \\ i_2 = -i_c \end{cases} \tag{6}$$

Substituting (3) into (6), it is gained,

$$\begin{aligned} j=0,&\begin{cases} i_1 = Icos(\omega_0 kT_s + \varphi) \\ i_2 = -Icos(\omega_0 kT_s + \frac{2\pi}{3} + \varphi) \end{cases} \\ j=1,&\begin{cases} i_1 = Icos(\omega_0 kT_s - \frac{\pi}{3} + \varphi) \\ i_2 = -Icos(\omega_0 kT_s + \pi + \varphi) \end{cases} \end{aligned} \tag{7}$$

The duration of the pulse currents can be expressed as,

$$\begin{cases} t_{00} = T_s - 2(t_{P1} + t_{P2}) \\ t_{01} = \frac{t_{00}}{4} \\ t_{02} = t_{01} + t_{P1} \end{cases} \tag{8}$$

where t_{00} is the duration of the zero vectors, t_{P1} and t_{P2} are the durations of the pulse currents, as illustrated in Fig. 3, and they can be further derived as,

$$\begin{aligned} j=0,&\begin{cases} t_{P1} = \frac{Ref_a - Ref_b}{2}\frac{T_s}{2} \\ t_{P2} = \frac{Ref_b - Ref_c}{2}\frac{T_s}{2} \end{cases} \\ j=1,&\begin{cases} t_{P1} = \frac{Ref_b - Ref_a}{2}\frac{T_s}{2} \\ t_{P2} = \frac{Ref_a - Ref_c}{2}\frac{T_s}{2} \end{cases} \end{aligned} \tag{9}$$

Substituting (9) into (8), it is obtained that,

$$\begin{aligned} j=0,&\begin{cases} t_{01} = \frac{1}{4}T_s - \frac{\sqrt{3}M}{8}cos(k\omega T_s - \frac{\pi}{6})T_s \\ t_{02} = \frac{1}{4}T_s + \frac{3M}{8}cos(k\omega T_s + \frac{\pi}{3})T_s \end{cases} \\ j=1,&\begin{cases} t'_{01} = \frac{1}{4}T_s - \frac{\sqrt{3}M}{8}cos(k\omega T_s - \frac{\pi}{6})T_s \\ t'_{02} = \frac{1}{4}T_s - \frac{3M}{8}cos(k\omega T_s + \frac{\pi}{3})T_s \end{cases} \end{aligned} \tag{10}$$

where t_{0x} and t'_{0x} relate to $Segment\ I$ and II, respectively, and x can be $1 \sim 6$. Substituting (7) and (10) into (5), it can be obtained,

$$\begin{aligned} I_{mn} = &\frac{\omega_0}{\pi}\frac{1}{m\omega_s + n\omega_0}\sum_{k=0}^{N-1} \\ &\Big\{Icos(k\omega_0 T_s + \varphi) \times A(t)\Big(\Big|_{t=t_{01}}^{t=t_{02}} + \Big|_{t=t_{05}}^{t=t_{06}}\Big) \\ &-Icos(k\omega_0 T_s + \frac{2\pi}{3} + \varphi) \times A(t)\Big(\Big|_{t=t_{02}}^{t=t_{03}} + \Big|_{t=t_{04}}^{t=t_{05}}\Big) \\ &+Icos(k\omega_0 T_s - \frac{\pi}{3} + \varphi) \times A(t)\Big(\Big|_{t=t'_{01}}^{t=t'_{02}} + \Big|_{t=t'_{05}}^{t=t'_{06}}\Big) \\ &-Icos(k\omega_0 T_s + \pi + \varphi) \times A(t)\Big(\Big|_{t=t'_{02}}^{t=t'_{03}} + \Big|_{t=t'_{04}}^{t=t'_{05}}\Big)\Big\} \end{aligned} \tag{11}$$

where $A(t) = sin[(m\omega_s + n\omega_0)t + n\omega_0(k + jN)T_s + \theta_{mn}]$. Considering $n\omega_0 \ll m\omega_s$ (I_{mn} with large n is much smaller than the dominant harmonics), $A(t)$ can be simplified as,

$$A(t) = sin[m\omega_s t + n\omega_0(k + jN)T_s + \theta_{mn}] \tag{12}$$

According to Fig. 3, it can be easily gained that,

$$\begin{cases} t_{01} + t_{06} = T_s \\ t_{02} + t_{05} = T_s \\ t_{03} + t_{04} = T_s \end{cases} \begin{cases} t'_{01} + t'_{06} = T_s \\ t'_{02} + t'_{05} = T_s \\ t'_{03} + t'_{04} = T_s \end{cases} \tag{13}$$

According to (12) and (13), it is obtained that,

$$\begin{aligned} &A(t_{06}) = A(-t_{01}), A(t_{05}) = A(-t_{02}), A(t_{04}) = A(-t_{03}) \\ &A(t'_{06}) = A(-t'_{01}), A(t'_{05}) = A(-t'_{02}), A(t'_{04}) = A(-t'_{03}) \end{aligned} \tag{14}$$

Another condition regarding to the time points is,

$$t_{01} + t_{03} = \frac{T_s}{2}, t'_{01} + t'_{03} = \frac{T_s}{2} \tag{15}$$

Substituting (15) into (12), it can be obtained that,

if m is odd,

$$\begin{aligned} &A(t_{03}) = -A(-t_{01}), A(-t_{03}) = -A(t_{01}) \\ &A(t'_{03}) = -A(-t'_{01}), A(-t'_{03}) = -A(t'_{01}) \end{aligned} \tag{16}$$

if m is even,

$$A(t_{03}) = A(-t_{01}), A(-t_{03}) = A(t_{01})$$
$$A(t'_{03}) = A(-t'_{01}), A(-t'_{03}) = A(t'_{01}) \quad (17)$$

According to (10), it is found that,

$$t'_{01} = t_{01}, \quad t'_{02} = \frac{T_s}{2} - t_{02} \quad (18)$$

Substituting (18) into (12), it is obtained that,

if m is odd,

$$A(t'_{02}) = -A(-t_{02}), \quad A(-t'_{02}) = -A(t_{02}) \quad (19)$$

if m is even,

$$A(t'_{02}) = A(-t_{02}), \quad A(-t'_{02}) = A(t_{02}) \quad (20)$$

Substituting (12), (14), (16), (17), (19) and (20) into (11), it can be gained,

if m is odd, $n = 3z$ and z is odd (otherwise $I_{mn} = 0$),

$$I_{mn} = \frac{\omega_0}{\pi} \frac{12}{m\omega_s + n\omega_0} \sum_{k=0}^{N-1} \Big\{ Icos(k\omega_0 T_s + \frac{\pi}{3} + \varphi) \times \Big[sin(m\omega_s t_{02}) - sin(m\omega_s t_{01}) \Big] cos(n\omega_0 k T_s + \theta_{mn}) \Big\} \quad (21)$$

if m is even, $n = 3z$ (otherwise $I_{mn} = 0$) and z is even,

$$I_{mn} = \frac{\omega_0}{\pi} \frac{12}{m\omega_s + n\omega_0} \sum_{k=0}^{N-1} \Big\{ \Big[Icos(k\omega_0 T_s + \frac{\pi}{3} + \varphi) \times sin(m\omega_s t_{02}) - \sqrt{3} Icos(k\omega_0 T_s - \frac{\pi}{6} + \varphi) \times sin(m\omega_s t_{01}) \Big] \times cos(n\omega_0 k T_s + \theta_{mn}) \Big\} \quad (22)$$

The magnitude of the harmonics in the DC link current is finally obtained by the following equations,

$$|I_{mn}| = \sqrt{I_{mn}^2(\theta_{mn} = 0) + I_{mn}^2(\theta_{mn} = \frac{\pi}{2})} \quad (23)$$

While the DC capacitor current can be gained as,

$$\begin{aligned} i_{cap} &= i_{dc1} - i_{dc2} = I_{01} - I_{02} + \\ &\sum_{n=1}^{\infty} \Big\{ |I_{n1}| cos[n\omega_{01}(t - t_0) + \theta_{n1}] - \\ &|I_{n2}| cos[n\omega_{02}(t - t'_0) + \theta_{n2}] \Big\} + \\ &\sum_{m=1}^{\infty} \sum_{n=-\infty}^{\infty} \Big\{ |I_{mn1}| cos[(m\omega_{s1} + n\omega_{01})(t - t_0) + \theta_{mn1}] - \\ &|I_{mn2}| cos[(m\omega_{s2} + n\omega_{02})(t - t'_0) + \theta_{mn2}] \Big\} \end{aligned} \quad (24)$$

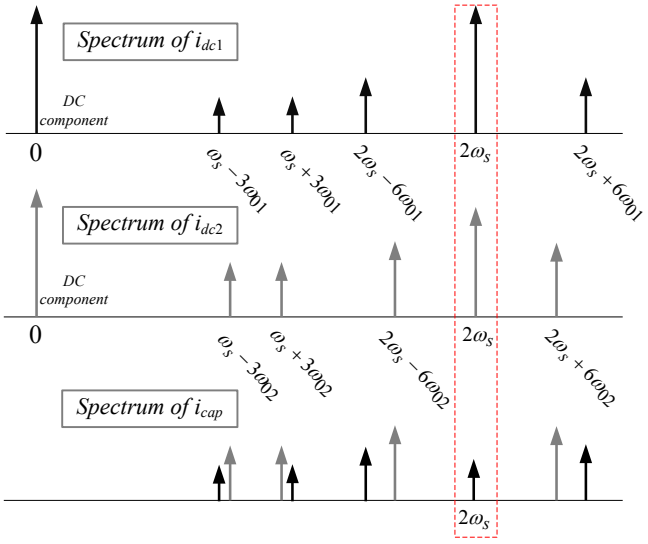

Fig. 4. The relationship between the Spectrum of the DC link current and the DC capacitor current.

where x_1 and x_2 represent the parameters of the rectifier and the inverter, respectively, and x can be i_{dc}, I_0, I_n, ω_0, θ_n, I_{mn}, ω_s, and θ_{mn}. t_0 and t'_0 are the initial time of the rectifier and the inverter, respectively. Since the input and output power of the BTB are balanced, the DC link current should have the same DC component. The active rectifier and the inverter normally have different fundamental frequencies such as in the motor drive application, the baseband and carrier-sideband harmonics thus are completely retained in the DC capacitor current. The carrier frequency can be easily made the same to cancel the harmonics at carrier frequency multiplier. The scheme is also illustrated in Fig. 4. Actually, the baseband harmonics of the DC link current are much smaller than the carrier frequency and carrier sideband harmonics, therefore they are neglected. It should be noted that the RMS value of carrier-sideband group can be calculated at the carrier frequency multiplier since their frequencies are quite close [13], but this is only valid for the DC capacitor current in a single stage converter and not the BTB converter.

The harmonics of carrier frequency multiplier can be obtained by substituting $n = 0$ into (22) and it is,

$$i_{m0} = I_{m0}(\theta_{m0} = 0) cos[m\omega_s(t - t_0)] \quad (25)$$

If the rectifier and the inverter have the same carrier frequency ($\omega_{s1} = \omega_{s2}$) and phase ($t_{01} = t_{02} + aT_s, a \in Z$), the harmonics of carrier frequency multiplier in the DC link current can be derived as,

$$I_{m0,cap} = I_{m01}(\theta_{m01} = 0) - I_{m02}(\theta_{m02} = 0) \quad (26)$$

III. The Current Spectrum

The impacts of the ac power factor angle φ, the fundamental frequency ω_0, and the modulation index M on the spectrum of the DC link current are investigated for a general voltage source inverter or rectifier based on the analytic expression and they are illustrated in Fig. 5, Fig. 6, Fig. 7 and Fig. 8.

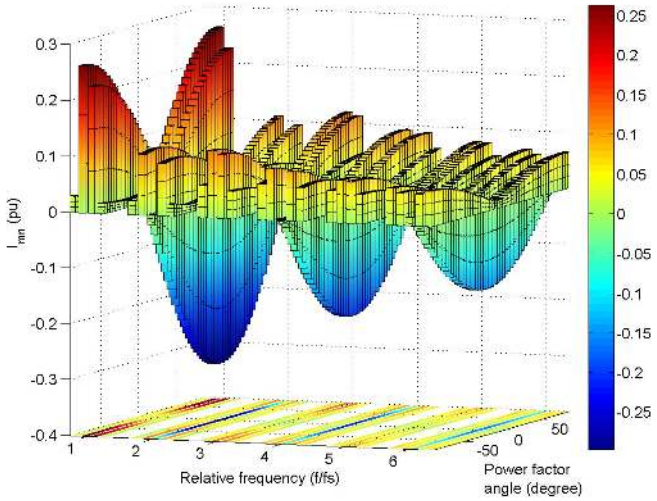

Fig. 5. Spectrum of the DC link current vs. phase angle ($M = 1$).

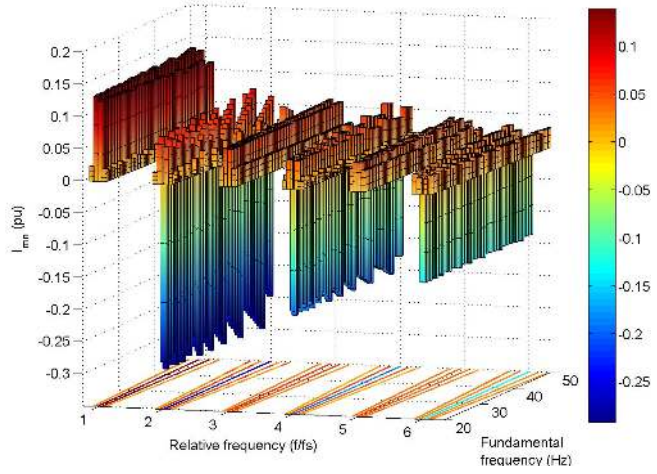

Fig. 6. Spectrum of the DC link current vs. fundamental frequency ($\varphi = \pi/6, M = 1$).

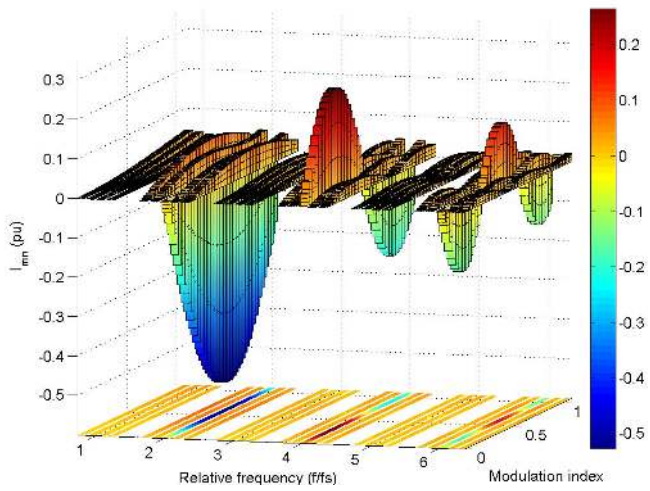

Fig. 7. Spectrum of the DC link current vs. modulation index ($\varphi = 0$).

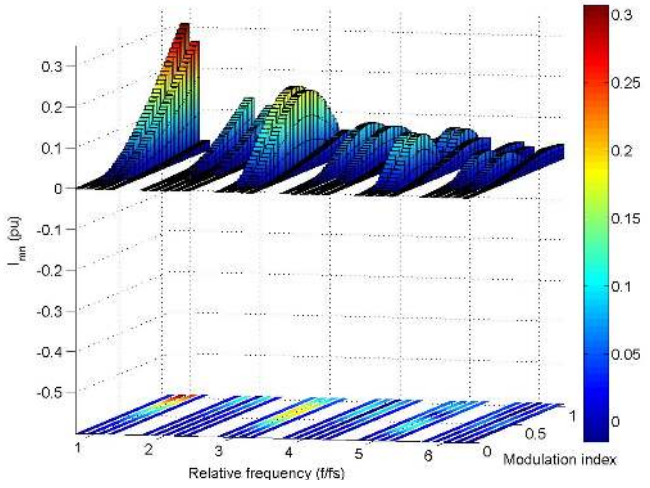

Fig. 8. Spectrum of the DC link current vs. modulation index ($\varphi = \pm\pi/2$).

The z-axis is I_{mn} when $n = 0$, otherwise it is $|I_{mn}|$. First of all, only even harmonics exist at carrier frequency multiplier. When φ is close to zero, all the carrier-sideband harmonics will also become zero, while the even carrier frequency harmonics achieve their peak values. However the carrier frequency harmonics will attenuate to zero when φ increases to $\pm\pi/2$, at the same time the carrier-sideband harmonics will increase (Fig. 5). The variation of the fundamental frequency only influences the spectrum slightly (Fig. 6). The carrier frequency harmonics will increase when the modulation index decreases from 1.1 to 0.7, which covers the normal operation range of the back-to-back converter. Meanwhile, the trends of the carrier sideband harmonics are inconsistent. The harmonics at $\omega_s \pm 3\omega_0$ will decrease while those at $3\omega_s \pm 9\omega_0$ will increase, which are the dominant components. Moreover, $\varphi = 0$ will lead to cancellation of the carrier-sideband harmonics and $\varphi = \pm\pi/2$ will cause zero carrier harmonics (Fig. 7 and 8).

In order to cancel the carrier frequency harmonics as much as possible, the impact of the phase shift between the two carriers on the DC capacitor current spectrum needs to be investigated. According to (36), it is obtained,

$$i_{m0,cap} = I_{m01}cos[m\omega_s(t-t_0)] - I_{m02}cos[m\omega_s(t-t_0')] \quad (27)$$

The initial time difference can be defined as,

$$t_0 - t_0' = aT_s + \Delta T, \quad a \in Z, -\frac{T_s}{2} < \Delta T \leq \frac{T_s}{2} \quad (28)$$

Substituting (40) into (39), it is gained that,

$$I_{m0,cap} = \sqrt{I_{m01}^2 - 2I_{m01}I_{m02}cos(m\omega_s\Delta T) + I_{m02}^2} \quad (29)$$

The spectrum of the DC capacitor current as a function of ΔT is indicated in Fig. 9 and Fig. 10, where f_{01} and f_{02} are the fundamental frequency of the rectifier and the inverter, respectively. It can be seen that both the carrier-sideband harmonics of the rectifier and the inverter exist in the DC capacitor current, and they have no relation to ΔT. Moreover, the carrier-sideband harmonic become much smaller when $\varphi_1 = \varphi_2$ changes from $\pm\pi/2$ to 0. To the contrary, the even

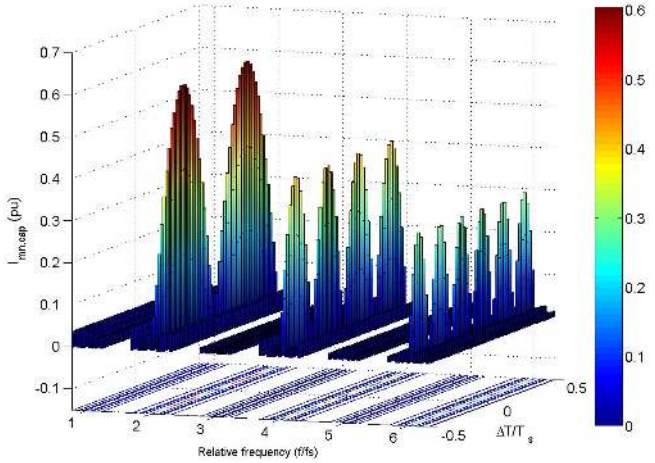

Fig. 9. Spectrum of the DC capacitor current vs. ΔT ($f_{01} = 50Hz, f_{02} = 31Hz, \varphi_1 = \varphi_2 = 0, M_1 = M_2 = 1, I_1 = I_2$).

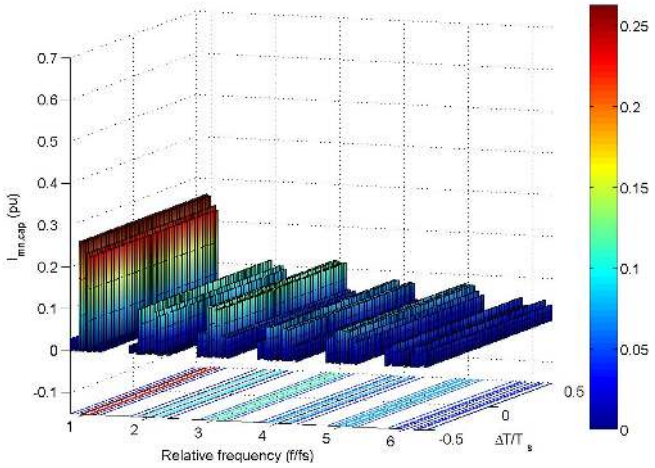

Fig. 10. Spectrum of the DC capacitor current vs. ΔT ($f_{01} = 50Hz, f_{02} = 31Hz, \varphi_1 = \varphi_2 = \pm\pi/2, M_1 = M_2 = 1, I_1 = I_2$).

carrier harmonics are close to zero when $\varphi_1 = \varphi_2 = \pm\pi/2$, and there is no odd carrier harmonic. Actually, the ΔT only have effect on the carrier harmonics in the DC capacitor current. When $\Delta T = 0$, all the even carrier harmonics achieve to zero, and then their amplitudes change periodically to the double of their frequency when $|\Delta T|$ increases.

As a conclusion of the analytic results above, from the DC capacitor current reduction point of view, the carriers of the rectifier and the inverter should be synchronized with each other not only the frequency but also the phase (actually the phase shift can be 0 or π). Then, considering the reality that the rectifier and the inverter normally have different modulation index M, phase shift φ, and ac current amplitude I, the effort to coordinate these parameters according to their impact on the spectrum of the DC link current is needed in order to make the spectrum of the DC link currents close to each other and thereby achieve a lower DC capacitor current. It should be kept in mind that, the I is only a gain of the harmonics, while both the M and the φ can lead to different trends of the carrier and the carrier-sideband harmonics.

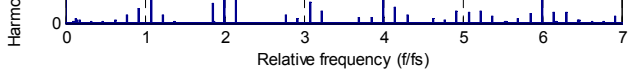

IV. Simulation Validation

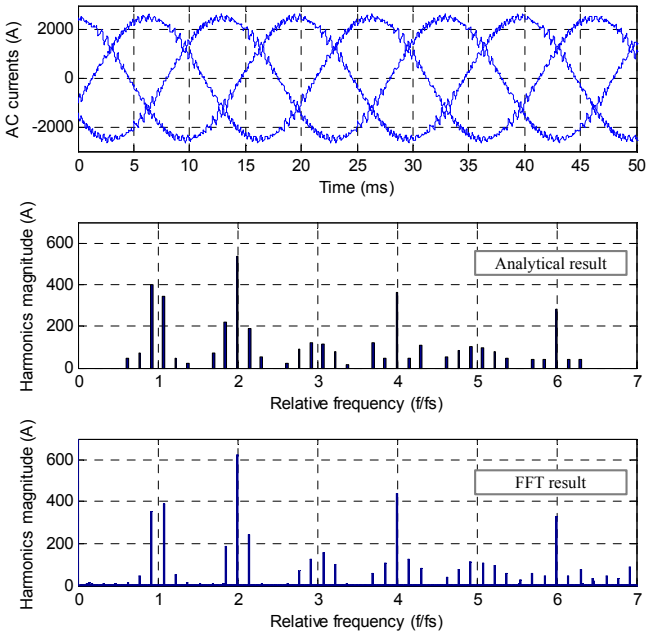

Fig. 11. The ac currents and the corresponding analytical and FFT spectrums (f_0 = 50 Hz, f_s = 2 kHz, $\varphi = -32^o$, M = 1.05, I = 2507 A).

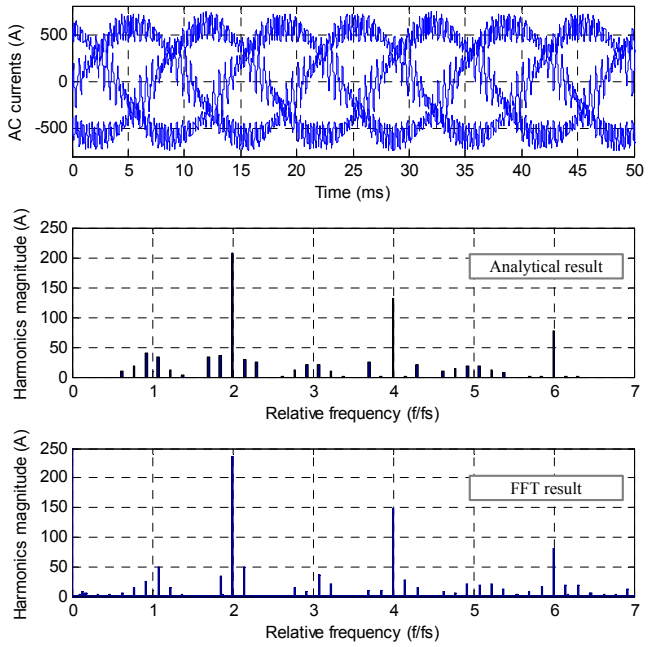

Fig. 12. The ac currents and the corresponding analytical and FFT spectrums (f_0 = 50 Hz, f_s = 2 kHz, $\varphi = -13^o$, M = 0.95, I = 606 A).

In order to verify the accuracy of the analytic expression of the DC link current spectrum, a BTB converter is built in *PLECS Blockset* and SVPWM is employed to keep consistent with the analysis. The Fast Fourier Transformation (FFT) function is used to obtain the DC link current spectrum. The comparisons between the spectrums gained by the analytic expression and FFT are carried out and they are shown in Fig.

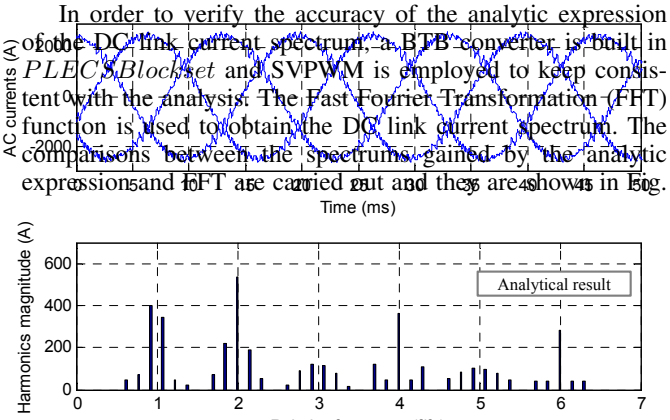

11 and Fig. 12 at two different power ratios. As seen, a good agreement of the dominant harmonics of the DC link current is achieved between the analytical and FFT results, in terms of the first carrier-sideband group, second carrier-sideband group, and the even harmonics of the carrier frequency. Moreover, the accuracy of the analytic expression is still acceptable with 30% ac current ripple, although the ripple is not considered in the derivation of the analytic expression.

V. Experimental Test

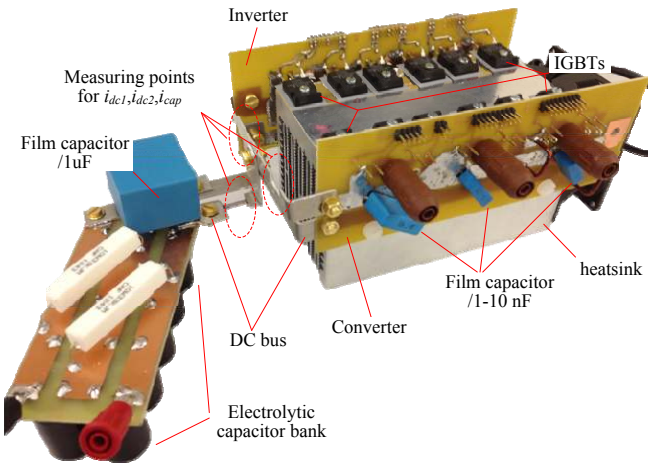

Fig. 13. The 1.5 kW back-to-back prototype for the validation.

In order to verify the analysis in Section II and III, a 1.5 kW back-to-back converter is built up, as shown in Fig. 13. The DC capacitors contain a 900 uF electrolytic capacitor bank and a 1 uF film capacitor, where the latter one is used to clamp the overshot of the dc bus voltage due to its much better performance at high frequency. Besides, a much smaller film capacitor is put on the dc bus close to each phase leg of both the rectifier and the inverter, in order to clamp the overshot of the dc bus voltage and protect the IGBTs. But since their capacitances (1 nF - 10 nF) are much smaller than the one with the capacitor bank, they will only draw the dc link current slightly. Thereby, the currents measured at the points as shown in Fig. 13 can be considered as the ideal i_{dc1}, i_{dc2}, and i_{cap}. The experiment results are indicated in Fig. 14 and Fig. 15, where the dc bus voltage is 250 V, the fundamental frequencies of the rectifier and the inverter are 50 Hz and 40 Hz, respectively, V_1 and V_2 are the amplitudes of the AC voltages and indirectly represent the modulation indexes of the rectifier and the inverter, PF_1 and PF_2 are their power factors. The phase voltage, power factor, and amplitude of the phase current of the inverter are always kept at 85 V, 1, and 8 A. It can be seen that when both the amplitudes of the phase voltage and power factors of the rectifier and the inverter are the same, the amplitudes of the DC-link currents i_{dc1} and i_{dc2} are quite close to each other (Fig. 14 (a)), where the small difference is due to the voltage drop on the inductor of the ac filter. The DC-link current amplitude of the rectifier will increase when its power factor or phase voltage decreases (Fig. 14 (b) and Fig. 14 (c)). Moreover, the DC-link currents i_{dc1} and i_{dc2} are always in-phase (Fig. 15 (a), (b) and (c)), because of the synchronization of the carriers. Besides, when the amplitudes of the phase voltage and power factors are the same, the rectifier and the inverter will have almost the same pulsed DC-link currents, in terms of the amplitude and width. Thereby, the capacitor current i_{cap} is minimized (Fig. 15 (a)). When the power factor of the converter decreases to 0.9 its DC-link current i_{dc1} will be slightly changed on the amplitude and also the width. At the same time, the capacitor current i_{cap} will increase slightly (Fig. 15 (b)). A larger change can be observed on the amplitude and width of dc-link current i_{dc1}, when the AC voltage of the converter decreases to 0.75 pu, and the capacitor current is also much larger than the other two cases (Fig. 15 (c)). The RMS values of the capacitor currents are calculated based on the measured data, and they are 1 pu, 1.3 pu and 1.8 pu (2.4 A is normalized as 1 pu) for the three cases in Fig. 15 (a), (b), and (c), respectively.

VI. Conclusion

New perspectives to reduce the DC-link capacitor ripple current have been investigated based on a generic derivation on the capacitor current ripple of the BTB converter. Besides the synchronization of the pulsed dc-link currents of the rectifier stage and inverter stage of BTB converter, the theoretical studies reveal that the width and amplitude of the pulsed dc-link currents also have significant impact on the capacitor current stresses. The factors which influence those width and amplitude are therefore identified, such as the modulation index and the power factor. A 1.5 kW BTB converter prototype is built and the DC-link capacitor ripple current is measured under different control conditions. The experimental results verify the theoretical expectations.

References

[1] H. Wang, M. Liserre, and F. Blaabjerg, "Toward reliable power electronics: Challenges, design tools, and opportunities," *IEEE Industrial Electronics Magazine*, vol. 7, no. 2, pp. 17–26, 2013.

[2] F. Blaabjerg, K. Ma, and D. Zhou, "Power electronics and reliability in renewable energy systems," *in Proc. of ISIE*, pp. 19–30, 2012.

[3] C. Busca, R. Teodorescu, F. Blaabjerg, S. Munk-Nielsen, L. Helle, T. Abeyasekera, and P. Rodriguez, "An overview of the reliability prediction related aspects of high power igbts in wind power applications," *Microelectronics reliability*, vol. 51, no. 9-11, pp. 1903–1907, 2013.

[4] H. Wang and F. Blaabjerg, "Reliability of capacitors for dc-link applications in power electronic converters an overview," *IEEE Trans. Ind. Appl.*, in press.

[5] J. Dai, D. Xu, and B. Wu, "A novel control scheme for current-source-converter-based pmsg wind energy conversion systems," *IEEE Trans. Power Electron.*, vol. 24, no. 4, pp. 963–972, 2009.

[6] J. Yao, H. Li, Y. Liao, and Z. Chen, "An improved control strategy of limiting the dc-link voltage fluctuation for a doubly fed induction wind generator," *IEEE Trans. Power Electron.*, vol. 23, no. 3, pp. 1205–1213, 2008.

[7] L. Gonzalez, G. Garcera, E. Figueres, and R. Gonzalez, "Effects of the pwm carrier signals synchronization on the dc-link current in back-to-back converters," *Applied Energy*, vol. 87, no. 8, pp. 2491–2499, 2010.

[8] B. G. Gu and K. Nam, "A dc-link capacitor minimization method through direct capacitor current control," *IEEE Trans. Ind. Appl.*, vol. 42, no. 2, pp. 573–581, 2006.

[9] J. W. Kolar, T. M. Wolbank, and M. Schrodl, "Analytical calculation of the rms current stress on the dc link capacitor of voltage dc link pwm converter systems," *in Proc. of IEEE-EMD*, pp. 81–89, 1999.

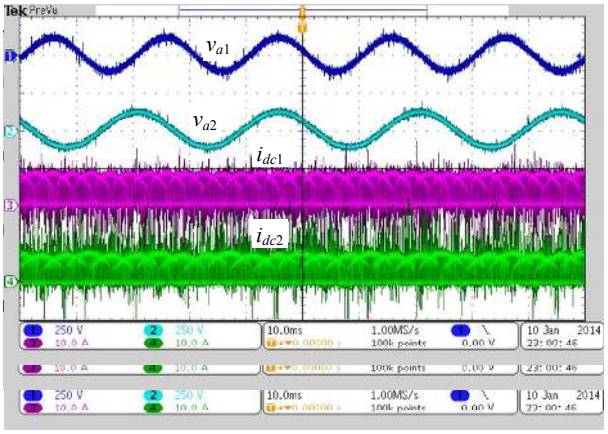

(a) V_1 = 1 pu, V_2 = 1 pu, PF_1 = 1, PF_2 = 1

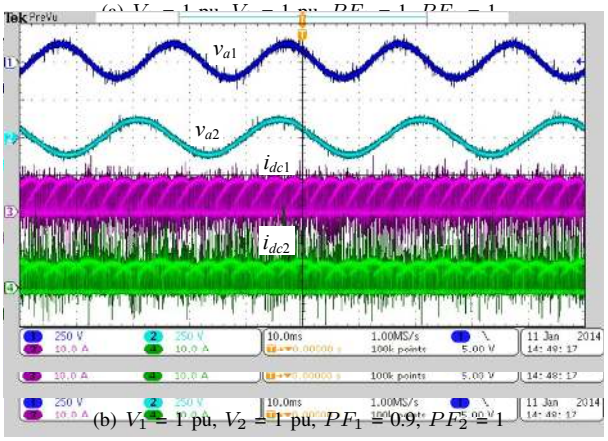

(b) V_1 = 1 pu, V_2 = 1 pu, PF_1 = 0.9, PF_2 = 1

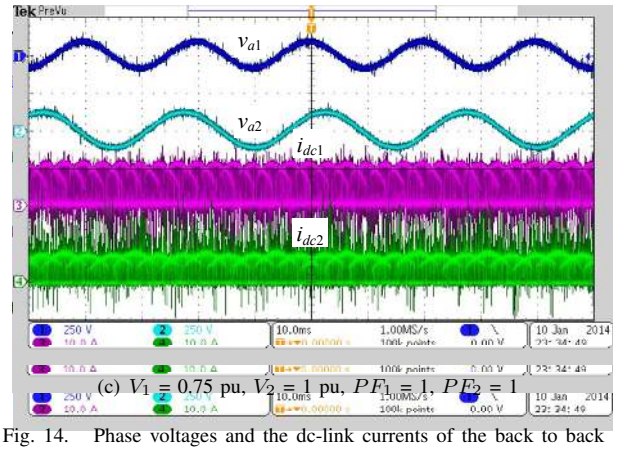

(c) V_1 = 0.75 pu, V_2 = 1 pu, PF_1 = 1, PF_2 = 1

Fig. 14. Phase voltages and the dc-link currents of the back to back converter.

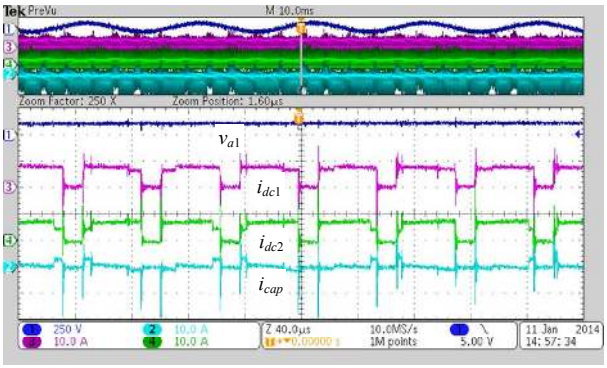

(a) V_1 = 1 pu, V_2 = 1 pu, PF_1 = 1, PF_2 = 1

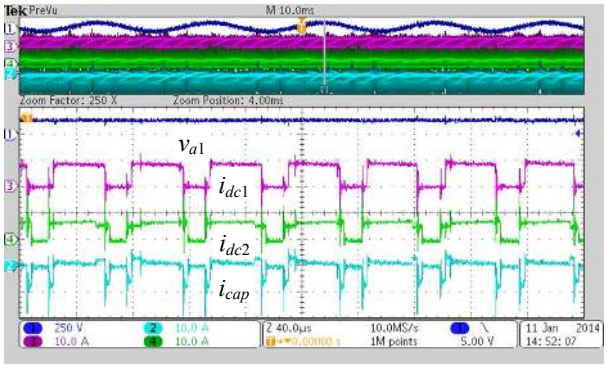

(b) V_1 = 1 pu, V_2 = 1 pu, PF_1 = 0.9, PF_2 = 1

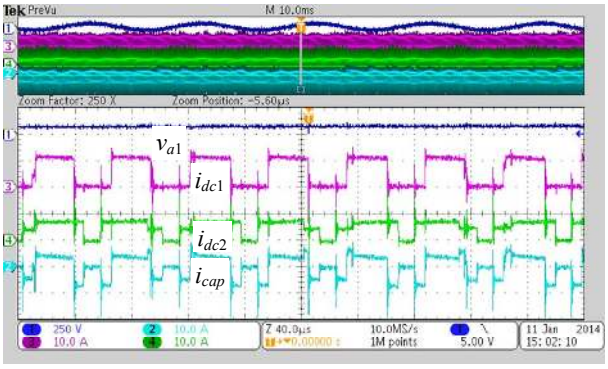

(c) V_1 = 0.75 pu, V_2 = 1 pu, PF_1 = 1, PF_2 = 1

Fig. 15. The dc-link currents and the ripple current of the dc-link capacitor of the back to back converter.

[10] D. G. Holmes and T. A. Lipo, "Pulse width modulation for power converters," *IEEE Press*, 2003.

[11] D. G. Holmes and B. P. McGrath, "Opportunities for harmonic cancellation with carrier-based pwm for two-level and multilevel cascaded inverters," *IEEE Trans. Ind. Appl.*, vol. 37, no. 2, pp. 574–582, 2001.

[12] B. P. McGrath and D. G. Holmes, "A general analytical method for calculating inverter dc-link current harmonics," *IEEE Trans. Ind. Appl.*, vol. 45, no. 5, pp. 1851–1859, 2009.

[13] U. Ayhan and A. M. Hava, "Analysis and characterization of dc bus ripple current of two-level inverters using the equivalent centered harmonic approach," *in Proc. of IEEE-ECCE*, pp. 3830–3837, 2011.

[14] F. D. Kieferndorf, M. Forster, and T. A. Lipo, "Reduction of dc-bus capacitor ripple current with pam/pwm converter," *IEEE Trans. Ind. Appl.*, vol. 40, no. 2, pp. 607–614, 2004.

[15] H. Wen, W. Xiao, X. Wen, and P. Armstrong, "Analysis and evaluation of dc-link capacitors for high-power-density electric vehicle drive systems," *IEEE Trans. Vehicular Technology*, vol. 61, no. 7, pp. 2950–2964, 2012.

[16] M. L. Gasperi, "Life prediction modelling of bus capacitors in ac variable-frequency drives," *IEEE Trans. Ind. Appl.*, vol. 41, no. 6, pp. 1430–1435, 2005.